The Astrophysical Journal, 640:1078–1085, 2006 April 1

THE WARPED CIRCUMSTELLAR DISK OF HD 100546

Alice C. Quillen
Department of Physics and Astronomy, University of Rochester, Rochester, NY 14627; and Research School of Astronomy and Astrophysics, Australian National University, Mount Stromlo Observatory, Cotter Road, Weston Creek, ACT 2611, Australia; aquillen@pas.rochester.edu
Received 2005 May 11; accepted 2005 November 30

ABSTRACT

We propose that the two-armed spiral features seen in visible *Hubble Space Telescope* images of scattered light in HD 100546's circumstellar disk are caused by the illumination of a warped outer disk. A tilt of 6°–15° from the symmetry plane can cause the observed surface brightness variations, providing the disk is very twisted (highly warped) at radii greater than 200 AU where the spiral features are seen. Dust lanes are due in part to shadowing in the equatorial plane from the inner disk within a radius of 100 AU. HD 100546's outer disk, if viewed edge-on, would appear similar to that of Beta Pictoris. A disk initially misaligned with a planetary system becomes warped due to precession induced by planetesimal bodies and planets. However, the twistedness of HD 100546's disk cannot be explained by precession during the lifetime of the system induced by a single Jovian-mass planet within the clearing at $\sim$13 AU. One possible explanation for the corrugated disk is that precession was induced by massive bodies embedded in the disk at larger radius. This would require approximately a Jupiter mass of bodies well outside the central clearing at 13 AU and within the location of the spiral features or at radii approximately between 50 and 200 AU.

Subject heading: stars: individual (HD 100546)

1. INTRODUCTION

High angular resolution imaging of circumstellar disks have shown that these disks may not be coplanar. For example, the disk of Beta Pictoris exhibits a warp; the outer disk at radii greater than 50 AU is tilted between 3° and 5° from the disk interior (Burrows et al. 1995; Heap et al. 2000). Models for the scattered optical light of the bowed disk of AU Microscopii suggest that this disk is also warped, with a small tilt of about 3° (Krist et al. 2005). While warped disks are easiest to identify in nearly edge-on systems such as Beta Pictoris and AU Microscopii, less inclined or nearly face-on disks may also not be coplanar. This leads us to search for features in less inclined disks that might also be explained with a warped disk model. As proposed by Mouillet et al. (1997) and Augereau et al. (2001b), the twistedness of Beta Pictoris's warped disk could be a result of precession induced by unseen planets or planetesimals residing in the disk. Consequently, by probing the geometry of the warp, we can constrain the properties of the unseen planetary system.

HD 100546 is a nearby southern Herbig Be star (B9.5 Ve; distance $d = 103 \pm 6$ pc) with an estimated age $t \sim 10$ Myr (van den Ancker et al. 1997) that exhibits a dusty circumstellar disk revealed in scattered light from visible and near-infrared imaging (Grady et al. 2001; Augereau et al. 2001a). We note that at the distance of HD 100546, $1''$ corresponds approximately to 100 AU. Most noticeable in the images of this disk taken by the *Hubble Space Telescope* (*HST*) using the Space Telescope Imaging Spectrograph (STIS) camera are the two nearly symmetrical spiral features at a radius of about 250 AU from the star (Grady et al. 2001). Quillen et al. (2005) showed that the two arms were unlikely to be caused by spiral density waves excited by a planet embedded in the disk but could be density variations pulled out tidally by a nearby passing star. However, Quillen et al. (2005) then ruled out this scenario for a number of reasons. To match the openness of the arms, the flyby had to be recent: within a few thousand years. Not only is the probability for this scenario extremely low, but it also implies that the perturbing object is near HD 100546. A search for a perturbing object (star) massive enough to account for the two arms was negative. Quillen et al. (2005) concluded that the spiral features were not density enhancements resulting from the tidal force of a recent stellar close encounter. In contrast, both Quillen et al. (2005) and Ardila et al. (2005) have shown that the spiral arms in the outer part of HD 141569A's disk *are* likely to have been pulled out tidally by the nearby passage of its binary companion, HD 141569B and C.

Warped disks can display complex morphology. Previous work modeling galactic warped disks (e.g., Quillen et al. 1992, 1993, 2006; Quillen & Bower 1999; Nicholson et al. 1992; Tubbs 1980; Steiman-Cameron et al. 1992) accounts for the optical dust lanes seen in Centaurus A and other galaxies and the parallelogram-shaped infrared morphology seen in *Spitzer* images of Centaurus A. These previous studies have shown that the apparent morphology of a warped disk can be sensitive to its optical properties (e.g., Krist et al. 2005) as well as to its geometry. For emitting optically thin disks, folds in the disk can appear brighter to the viewer than other regions (see Quillen et al. [2006] and associated simulations). Likewise, we expect that optically thin disks appear brighter in scattered light in regions where the disk tilts at high inclination with respect to the viewer. This is because the surface brightness of an optically thin medium of uniform thickness that scatters light from a distant source is dependent on its orientation angle with respect to the viewer. We note that a disk that is optically thin when viewed from above (integrated vertically) may be optically thick when viewed edge-on. Folds in a warped disk could also be optically thick (as explored in the case of Centaurus A in the near-infrared; Quillen et al. 1993).

Here we consider the possibility that the disk of HD 100546 is warped and that the warp is responsible for the observed spiral features. We first consider the case in which the outer disk is isotropically illuminated by the central star. If the disk at large

radii is warped and optically thick, then we would expect that the optical images would exhibit only one spiral arm. Only the high side of the disk would be illuminated, whereas the opposite side would be in shadow. If the disk is optically thin (even at folds) and warped at radii greater than 2″ or 200 AU, then we expect to see two spiral features. Regions of high inclination with respect to the viewer would appear brighter and would be located on opposite sides of the star.

We now consider the situation of a warped disk that is not isotropically illuminated. We expect that starlight illuminating the outer disk should be highly attenuated in the equatorial plane. A warped disk can be described as a series of rings. At each radius an inclined disk crosses the equatorial plane at two opposing points. Consequently, the shadow from the inner disk could cause two spiral dust lanes or shadows in the outer warped disk, resulting in the appearance of two spiral features. If the spiral features are due to an equatorial shadow, then the outer disk could be either optically thin or thick. If the outer disk is optically thick, then one would expect two spiral shadows and one bright spiral feature, whereas if the outer disk is optically thin, then one would expect two spiral shadows with brighter spiral features lying between them.

Unfortunately, it is not straightforward to estimate the disk normal optical depth and width of HD 100546's disk as a function of radius. Based on the near-IR scattered light surface brightness, Pantin et al. (2000) estimated that the disk has a high normal optical depth, $\tau \sim 1$, at radii greater than 1″ or 100 AU. Augereau et al. (2001a) estimated a normal optical depth 40–50 times lower, suggesting that the outer disk is optically thin at optical and near-IR wavelengths outside of ~80 AU. However, the scattered stellar light is likely to be obscured at large radii in the midplane, and this would cause an underestimate in the disk normal optical depth at large radii (Augereau et al. 2001a). The observed infrared spectral energy distribution of HD 100546 implies that the luminosity of emission from dust is large, 50% of the stellar photospheric luminosity. Most of the disk luminosity, 70%, is emitted in the mid-infrared and so from a radius ~10–20 AU (Bouwman et al. 2003), well within the location of the spiral features at ~250 AU in scattered light. The estimated radius of the mid-infrared emission based on the spectral energy distribution is approximately consistent with mid-infrared high angular resolution observations (Liu et al. 2003). The infrared spectral energy distribution can be explained with a disk containing an inner, puffed-up region absorbing and reradiating half of the stellar light, accounting for the large mid-infrared flux. Because of its large covering angle, the puffed inner disk edge shades the outer disk (Bouwman et al. 2003; Dullemond et al. 2001; Dullemond & Dominik 2004). However, this model implies that the disk greater than 1″ or 100 AU, which has been observed in scattered light, is illuminated by the starlight that must pass first through the inner puffed-up region of the disk. This situation makes it challenging to estimate the optical depth of the disk from the scattered light at radii greater than 1″.

In this paper we search for warped disk models that can account for the spiral features seen in HD 100546's disk. Warped disk models have some advantages over other models. Because planetary systems are nearly Keplerian, orbit orientations vary extremely slowly. Consequently, a warp can be maintained for many rotation periods. This eliminates one of the problems of the previously proposed transient spiral structure model. Edge-on systems such as Beta Pictoris, which are clearly warped, suggest that less highly inclined systems such as HD 100546 could also be warped. In § 2 we describe how we represent the geometry of a warped disk. We then explain how we synthesize model surface brightness images that can be compared to the observations. In § 3 we discuss dynamical or physical models for the disk warp based on the geometric model that best matches the observed disk morphology. A summary and discussion follows.

2. WARPED DISK MODELS

2.1. *Warp Geometry*

We first discuss our notation for describing the orientation of the planetary system with respect to the viewer. The orientation of a coplanar planetary system requires two angles to describe: χ, corresponding to the position angle (counterclockwise from north) of the axis of disk rotation on the sky, and an inclination angle, ϑ, that describes the tilt of this axis with respect to the line of sight. If ϑ is zero, then the planetary system is viewed face-on. For a system that is not coplanar, χ and ϑ refer to the orientation of the rotation axis corresponding to the total angular momentum of the system's disk and planets.

We describe the warped disk with respect to the rotation axis of the planetary system. A warped disk undergoing circular motion can be described as a series of rotating tilted rings, each with a different radius, r. The orientation of each ring is specified by two angles, a precession angle, $\Omega(r)$, similar to the longitude of the accenting node, and an inclination angle, $i(r)$. These angles are given with respect to the rotation axis of the planetary system and the direction of the line of sight. We measure the angle Ω from a reference line in the system's ecliptic plane (that perpendicular to the rotation axis). As viewed on the sky, this line lies on the rotation axis of the system but is projected onto the system's ecliptic plane. Our precession angle is the angle (measured at the star) between this line and the point at which the ring crosses the system's ecliptic plane. This is similar to the longitude of the ascending node, which is measured with respect to the vernal equinox and the point at which the orbit crosses the ecliptic.

2.2. *Constructing a Model Scattered Light Image*

To produce a model image of the optical scattering light, all reflecting and absorbing regions along the line of sight at each position on the sky must be considered. When the disk is optically thin, multiple scattering events and absorption can be neglected. In this case, each photon originates from the star and is then reflected from a single spot on the disk. At each position on the sky we can sum the reflected light at each location in the disk along the line of sight. We have restricted this modeling effort to an optically thin outer disk, at radii outside of 80 AU. However, we must keep in mind that future modeling efforts may need to consider outer disks with higher optical depth.

We begin by randomly sampling (x, y)-positions in the plane perpendicular to the disk rotation axis. At each position we compute a disk plane z-coordinate based on our assumed function for the precession and inclination angles $\Omega(r)$ and $i(r)$. To account for the disk thickness we add a vertical offset to z that was randomly chosen from a Gaussian distribution function. For the vertical structure of the disk we assume a normal distribution,

$$\rho(z) \propto \exp(-z^2/2h^2), \quad (1)$$

where h is the standard deviation of the distribution. The FWHM of this distribution is $2.35h$. We adopt a disk aspect ratio, h/r, that is independent of radius.

The coordinates of the (x, y, z)-position (in coordinates defined by the disk rotation axis) are then rotated using χ and ϑ to account for the orientation of the system rotation axis with respect to the viewer. To produce each model image, 200,000 points in the disk are sampled. Scattered starlight from these points are summed along each line of sight to produce a surface brightness image on the sky. The brightness of each point in the disk depends on the assumed albedo times the normal optical depth of that portion of the disk multiplied by the flux from the star at that position. The scattering amplitude of the reflected light from each point in the three-dimensional model was modified by the Henyey-Greenstein scattering phase function. The scattering asymmetric parameter, g, describes the scattering anisotropy ($g = 0$ corresponds to isotropic scattering, $g = 1$ to fully forward scattering). However, we do not vary g but instead adopt a fixed value of $g = 0.5$. We chose a representative value for g because of the uncertainty in the dust grain distribution and composition and because of the broadness of the filter used for the *HST* observations.

We take into account absorption of starlight from the inner disk by attenuating the starlight reaching the outer disk. We use an axisymmetric attenuation function that depends on the spherical coordinate, θ, where $\sin\theta = z/r$. We assume that the opacity of the inner disk

$$\tau_d(\theta) = \tau_0 \exp\left(-|\theta|/\theta_\tau\right), \tag{2}$$

where τ_0 is the opacity in the equatorial plane and θ_τ describes an angular scale length. Approximately 35% of the total stellar luminosity is absorbed by the inner disk at a radius of $\sim$10 AU (Bouwman et al. 2003). An opaque torus blocking 35% of the light would cover angles $-20^\circ < \theta < 20^\circ$. Because the star is a B9.5 V star, its spectrum is quite blue. Consequently, we expect $\tau_d \gtrsim 1$ at broadband optical wavelengths for angles somewhat smaller than the $\theta \sim 20^\circ$ required to block 35% of the total stellar luminosity.

Because the disk surface brightness is observed to drop $\propto r^{-3}$ within 2.″5 of the star (Grady et al. 2001; Augereau et al. 2001a), the disk normal optical depth must depend on radius. Taking into account the r^{-2} flux from the star, we match the observed radial drop with a -1 radial power in the normal optical depth (Augereau et al. 2001a). The normal optical depth times the albedo is taken to be a power-law function of radius, $\propto r^{-1}$. We note that if there are large variations in the disk orientation, then a different radial function may provide a better fit to the surface brightness profile of scattered light.

2.3. *The Precession Angle*

If the warp is due to the tidal force of a planet interior to the disk, then the precession rate of the longitude of the ascending node is approximately

$$\dot{\Omega}(r) \approx -\frac{3}{4} n \left(\frac{M_p}{M_*}\right)\left(\frac{D}{r}\right)^2, \tag{3}$$

as discussed by Mouillet et al. (1997). This approximation is appropriate for particles at low inclinations and in nearly circular orbits. Here n is the mean motion of the disk at radius r (equivalent to the angular rotation rate for a circular orbit), D is the semimajor axis of the planet, M_p is the mass of the planet, and M_* is the mass of the central star. This precession rate is appropriate in the limit for $D \ll r$ and is independent of the disk inclination. This precession rate also neglects the self-gravity of the disk and so is only appropriate when the disk is low mass.

TABLE 1
Common Parameters Describing the Warp Models

Parameter	Value
χ	40 (deg)
A_0	-260 (deg)
r_0	250 AU
Ω_0	230 (deg)
β	3.5

Notes.—The models shown in Figs. 1, 2, 3, and 4 have these parameters in common. The position angle of the system rotation axis on the sky is denoted by χ. The precession angle at the reference radius r_0 is Ω_0. The reference radius r_0 is given in AU (100 AU $\sim$1″ on the sky for HD 100546). The parameters A_0 and β describe the sensitivity of the precession angle Ω with radius or the twistedness of the warp; see eq. (4). The angles χ, Ω_0, and A_0 are given in degrees.

After a time Δt, an initially flat disk will have a precession angle,

$$\Omega(r) = \Omega_0 + A_0\left[\left(\frac{r}{r_0}\right)^{-\beta} - 1\right], \tag{4}$$

where Ω_0 is the precession angle at a reference radius, r_0. When the precession is due solely to a single distant planet, the constant

$$A_0 = -\frac{3\sqrt{GM_*}D^2\Delta t}{4r_0^{\beta}}\left(\frac{M_p}{M_*}\right), \tag{5}$$

and $\beta = 3.5$, corresponding to precession angle $\Omega \propto r^{-7/2}$. However, if there are multiple planets in the disk or the disk itself contains mass, one may consider more general laws or power laws with $\beta < 3.5$. In our numerical exploration we have explored variations in Ω_0, β, and A_0 to match the observed morphology of HD 100546's disk.

If a planet internal to the disk is initially taken out of the plane containing the disk, then the tilt angle i (with respect to the plane containing the planet) decreases with increasing radius (the situation considered by Mouillet et al. [1997]). However, if the disk itself is tilted via tidal forces from an external stellar encounter, then i would increase with increasing radius. Consequently, we allow the disk tilt angle, $i(r)$, to vary slowly with radius. At small radii where structure in the disk is difficult to resolve, models of the form given by equation (4) predict extremely tight corrugations. We let i drop to zero at small radii, so that tight corrugations in the inner region were removed from the model images. This allowed us to keep a simple power-law form for the precession angle. We allowed the inclination to vary with radius smoothly by using a spline function specified at four different radii, $r = 0$, 100, 200, and 400 AU. The inclination at $r = 0$ was set to 0°.

Common parameters for models are listed in Table 1. Parameters varied for individual models are listed in Table 2. We first attempt to match the morphology of the disk with a geometric

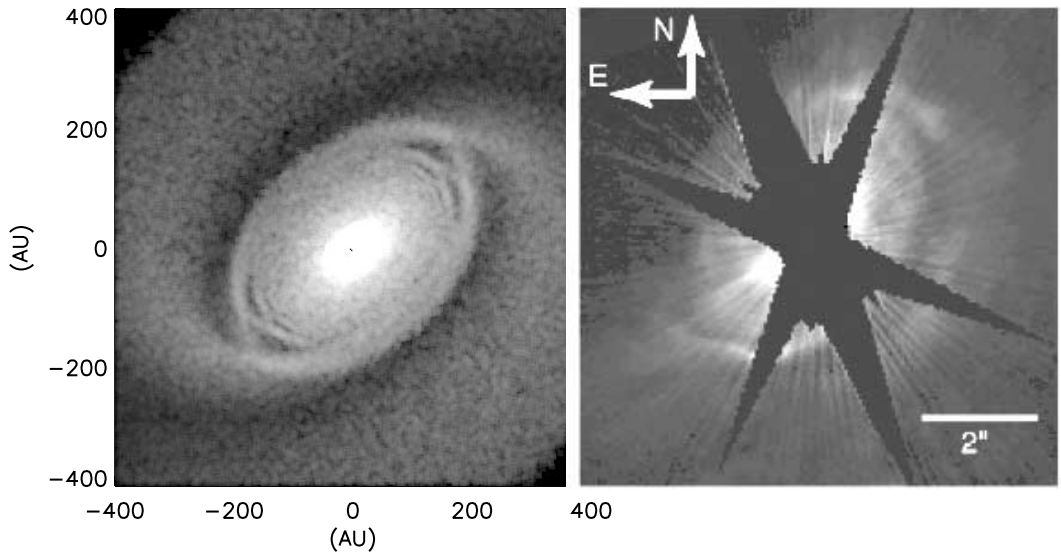

FIG. 1.—*Left*: Log surface brightness of model warped disk; MA with parameters are given in Tables 1 and 2. *Right*: Log of the surface brightness of the *HST* image of HD 100546 from Grady et al. (2001). Our model shows that a warped disk can exhibit surface brightness variations in a two-armed spiral pattern. The surface brightness variations are due to the slope or gradient changes in the disk surface with respect to the line of sight and an equatorial shadow from an inner disk.

model and then discuss physical models that can account for the observed geometry.

3. MODEL DISKS

In Figure 1 we show a model warped disk in comparison to the STIS image HD 100546 from Figure 1*e* by Grady et al. (2001). The parameters used to describe this model are listed in Table 1 and as model MA in Table 2. The rings comprising the disk are projected onto the sky in Figure 2. From a comparison of Figure 2 and Figure 1, we see that locations where the rings are in close proximity correspond to regions of higher surface brightness. These are regions where the disk slope or surface gradient (with respect to the line of sight) is high. Shadows from the inner disk are seen along the ring minor axes.

Surface brightness profiles for model MA along the major and minor axes, at position angles 127° and 37°, are shown in Figure 3. We compare our model surface brightness profiles with the major-axis profile shown in Figure 5*a* by Grady et al. (2001) of the STIS image. In both our model and the observed disk, one spiral feature corresponds to a bump in the major-axis surface brightness profile on the northwestern side at about 300 AU from the nucleus. The bump in the surface brightness profile is about 0.2 in the log above a smoothly dropping curve, approximately consistent with that seen in the observed profile. The increase in surface brightness corresponding to the opposite spiral feature is much less prominent on the southeastern side in both model and observed profile than that on the northwestern side.

Dust lanes are not prominent in the major-axis surface brightness profile (in either model or observed profiles); however, they are prominent in the model minor-axis profile. The dips in the major-axis profile exhibited by our model in Figure 3*a*, corresponding to dust lanes, are deeper than those observed. The dust lane on the southwestern side of the star is evident in the

TABLE 2
PARAMETERS DESCRIBING THE INDIVIDUAL MODELS

Parameter	MA	MB	MC	MD	ME
ϑ (deg)	52	52	52	52	89
i (deg)	3, 6, 15	3, 5, 20	6, 6, 6	3, 6, 15	3, 6, 15
h/r	0.05	0.05	0.05	0.08	0.05
τ_0	3.0	3.0	3.0	5.0	3.0
θ_τ (deg)	12.0	12.0	12.0	5.0	12

NOTES.—The inclination of the system rotation axis with respect to the viewer is ϑ. The inclination of the warped disk with respect to the system rotation axis is i. The angles ϑ and i are given in degrees. The disk aspect ratio, assumed to be constant with radius, is denoted by h/r. The standard deviation of the vertical density distribution is h, and the FWHM is $2.35h$. Inclination angles are given at three radii, $r = 100$, 200, and 400 AU, and we set $i = 0$ at $r = 0$. A spline function was fitted between these values. The opacity τ_0 describes the opacity of the inner disk in the equatorial plane. The parameter θ_τ describes the angular scale height of the inner disk's opacity in degrees. Surface brightness profiles, projected rings, and images for model MA are shown in Figs. 1, 2, and 3. Images are shown in Fig. 4 for models MB–ME.

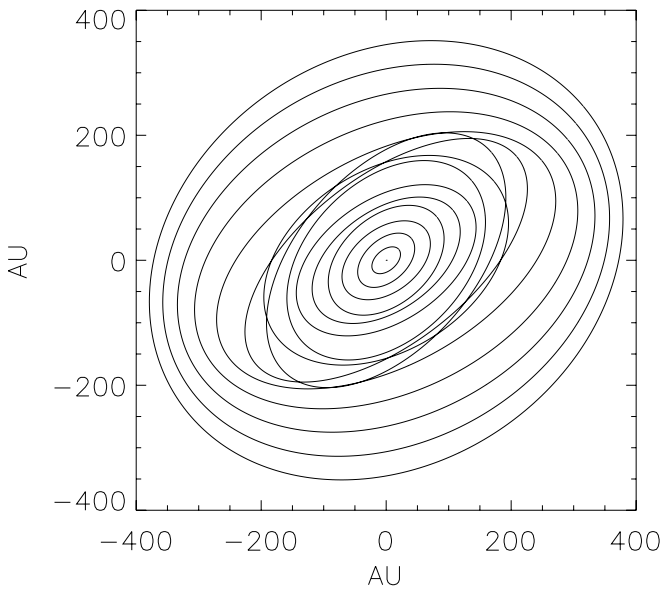

FIG. 2.—Projected circular disk rings at evenly spaced radii corresponding to the disk shown in Fig. 1 and described by model MA. Regions where projected rings are in close proximity, corresponding to regions of bright surface brightness (see Fig. 1). This is because these regions have large slopes or surface gradients with respect to the line of sight. The equatorial shadow lies along the minor axes of the rings.

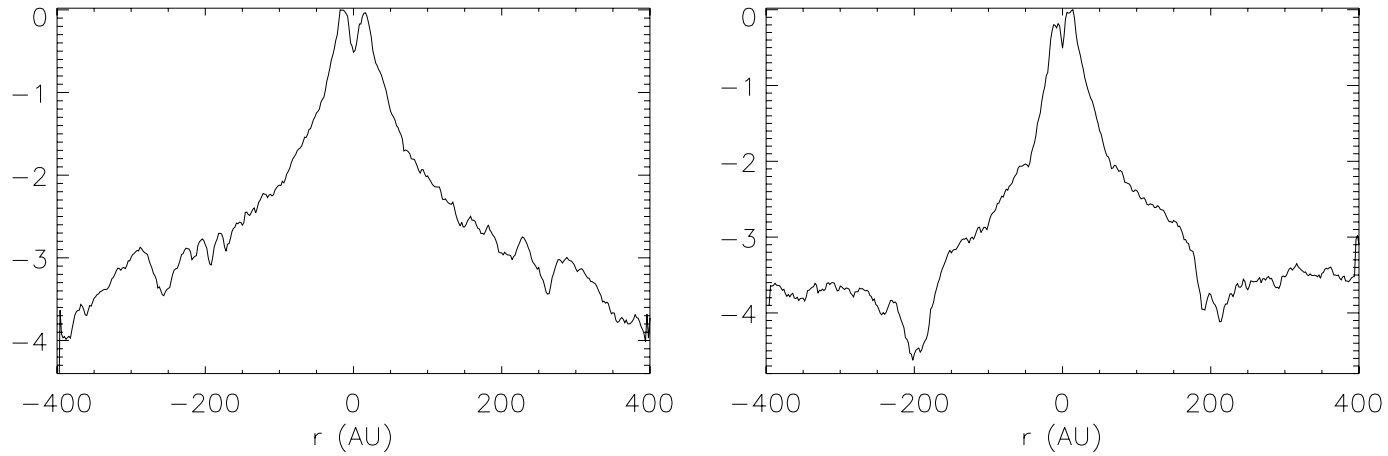

FIG. 3.—Major- and minor-axis surface brightness profiles for model MA, which is also shown in Figs. 1 and 2. Dips in the surface brightness profile are seen where there are dark dust lanes due to equatorial shadowing by the inner disk. Along the major axis at about 300 AU, an increase in the surface brightness is seen at a fold in the disk. A hole at $r = 13$ AU has been placed near the star, primarily to limit the flux range covered by the plot. For the major-axis profile, positive r refers to southeastern side of the disk. For the minor-axis profile, positive r refers to the near, or southwestern side of the disk. The y-axis shows $\log_{10}$ of the surface brightness normalized to the peak value.

STIS image by Grady et al. (2001), but there may not be a dust lane on the opposite, northeastern side of the disk. The model dust lane on the southwestern side is deeper than that on the northeastern side (see Fig. 3*b*). This asymmetry is probably due to anisotropic scattering in the model. The asymmetry in the strength of the opposing dust lanes is consistent with the observed image (there is a dust lane on the southwestern side but not necessarily on the southeastern one). Equatorial shadowing in the model is more extreme than that observed. We discuss this problem in more detail in § 3.1. The southern side of the disk is brighter than the north side because we allowed the scattering to be anisotropic and have taken the southern side to be nearer the viewer than the northern side. Some anisotropy in the scattering is consistent with the excess surface brightness in the near-infrared seen on the southern side at $r \sim 3''$ reported by Augereau et al. (2001a).

We find that a warped model, such as model MA shown in Figures 1–3, can provide a good explanation for the spiral features observed in the disk of HD 100546. The warp causes apparent surface brightness variations along two tightly wound spiral features, with darker regions within them. The darker regions were described as lanes by Grady et al. (2001). Two effects can account for regions of lower surface brightness: these regions are less inclined or more nearly perpendicular to the viewer (more nearly face-on), or they lie in the equatorial plane and so can be in the shadow of the inner disk. Higher surface brightness regions are those that rise above the midplane shadow. They also correspond to regions that have a steeper surface gradient or slope in the disk due to corrugations in the disk. Low inclination, evenly illuminated warps can exhibit large spatial variations in the scattered light surface brightness; however, this only occurs if the disk is highly corrugated or twisted and the disk is not optically thick.

In Figure 4 (*bottom right*), we show a nearly edge-on model ME, with parameters listed in Tables 1 and 2. This model is identical to model MA, shown in Figures 1–3, except the system is more highly inclined. Model ME can be compared to the edge-on disk of Beta Pictoris. Beta Pictoris is less twisted in its outer region compared to this model and does not have a shadow in its midplane. The one-planet model of Mouillet et al. (1997) would lead us to expect that the disk is more highly twisted at smaller radii. In future we may consider the possibility that some of the unresolved structure in Beta Pictoris's or AU Microscopii's inner disks at visible wavelengths might be explained with a warp that extends to smaller radii. We note that asymmetries between emission from one side of the disk compared to the opposite side would be introduced because the optical depth could be higher at folds and because of asymmetry due to anisotropic scattering.

3.1. *Sensitivity to Parameters*

In Figure 4 we show the effect of varying some of the parameters used to describe the disk. Model MA has a disk inclination

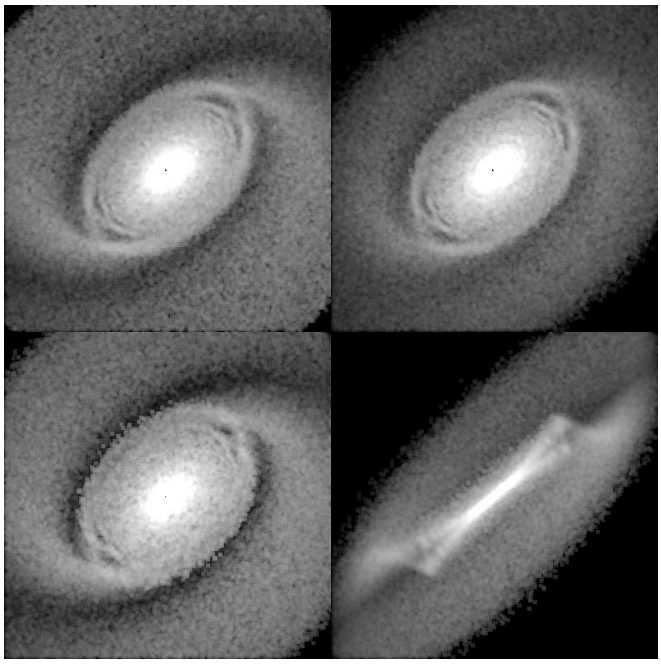

FIG. 4.—Effect of varying warped disk parameters. These models are similar to that (model MA) shown in Figs. 1, 2, and 3. Varied parameters are listed in Table 2. On the top left is model MB, which has a higher inclination at large radii than model MA. The top right panel shows model MC, which has constant inclination with radius. The bottom left panel shows model MD, which has a higher equatorial opacity for inner disk (larger τ_0) than model MA but a lower inner disk opacity angular scale height (θ_τ). On the bottom right, we show a nearly edge-on disk, model ME, to illustrate the extent of the twist and for comparison to edge-on systems such as Beta Pictoris.

that increases with increasing radius. When the inclination is held constant, as is true in model MC, shown in Figure 4 (*top right*), the spiral arms do not extend as far to the southwest and northeast as is seen in the observed scattered light image. We find that the angular extent of each spiral feature is smaller than that observed if i is held fixed. If the inclination with respect to the system axis increases with radius, then the spiral features extend over a larger range of angles, as shown in model MB in Figure 4 (*top left*). Model MB has an even higher outer inclination than model MA. Disks with larger tilts (larger i) tend to produce higher surface brightness variations in the spiral arms. However, if i is increased past 10°, then the disk can be folded with respect to the viewer, and this reduces the contrast of the spiral features. Models MA and MB have regions where multiple folds of the disk are encountered along the line of sight (see Fig. 2), and only the fold edges are regions of high surface brightness.

It is interesting to note that the apparent ends of the two spiral arms are about 180° apart and oriented nearly along the major axis of the disk. Such a situation arises naturally from the warped models. In contrast, spiral arms that are due to spiral density waves are not expected to end at locations 180° apart. The folds of the warped disk cause high surface gradient regions (corresponding to higher surface brightness regions) on either side of the nucleus. However, along the major axis these folds are oriented along the line of sight. As a result, spiral features in the model scattered light images tend to end along the disk major axis. Higher resolution models show a nested series of self-similar spiral features inside the outermost ones. This follows, since we have adopted a power-law form for the precession angle.

Similar morphology to that exhibited by model MA is seen when the inner disk has a higher equatorial opacity τ_0 but a shorter opacity angular scale length θ_τ. Model MD shows such a model. This model has a slightly larger outer disk scale height, which has the effect of smoothing the model surface brightness image. Had we left the disk scale height similar to that of model MA, this model would have had extreme contrast in its dust lanes. We find that thinner disks have more sharply defined spiral features and deeper dust lanes. When the angular scale length of the equatorial shadow is shorter (θ_τ is smaller), the dust lane is more sharply defined. Higher equatorial inner disk opacity (large τ_0) causes deeper shadows.

As we commented in § 3, we suspect that model MA has deeper dust lanes than observed. The equatorial shadow for model MA has an opacity of 1 (at visible wavelengths) at equatorial angles $\theta = \pm 13^\circ$. This opacity is sufficiently high so that it is approximately consistent with the absorption of ~35% of the stellar light from the inner disk. However, this high opacity and large angular scale length (in the inner disk opacity) implies that the outer disk is illuminated by visible light that has been significantly attenuated by the inner disk; much of the outer disk has a tilt lower than 13°. Our model computes the surface brightness at one wavelength only, corresponding to a central optical wavelength for the broad STIS image. It may be possible to improve the model image by integrating and summing images at different wavelengths. It is also possible that wings of the stellar point-spread function have smoothed the appearance of the outer disk, reducing the actual surface brightness contrast. The depth of the dust lanes in our model images can be decreased by increasing the angular scale length of the shadow, θ_τ. However, then the model midplane opacity must be reduced to reproduce the observed morphology. A midplane opacity below 1 would be unrealistic, as we expect the midplane to be dense and optically thick at visible wavelengths. To improve the model, we suspect that we would require a more complex function for the shadow than that given by equation (2). This function would necessarily be described by a larger number of parameters. A more complex model is difficult to constrained with the STIS image but could be constrained by future high-quality and multiwavelength images.

The twistedness of the disk is set by A_0. Higher $|A_0|$ corresponds to more highly wound spiral features. However, variations in A_0 can also change the radius of the spiral features if the radius r_0 is not simultaneously adjusted. Because the spiral features are tightly wound, we could not place constraints on the parameter β, which sets the dependence of α on radius; consequently, we set $\beta = 3.5$, consistent with the model explored by Mouillet et al. (1997). The contrast between the surface brightness on the near side compared to that on more distant side is larger if the scattering is more anisotropic (i.e., the scattering asymmetry parameter g is larger).

We find that only relatively thin outer disks, $h/r \lesssim 0.15$, have sufficiently sharp or fine features to be similar to the observations. The exponential scale height of the self-shadowed disk models by Dullemond (2002) and Dullemond & Dominik (2004) are lower than this (they exhibit drops in the density by a factor of 10 across $h/r \sim 0.1$ at radii of ~100 AU, as found from examination of Figures 2*b*, 3*b*, and 4*b* by Dullemond & Dominik [2004] and Figure 6 by Dullemond [2002]).

Here we have assumed a simple power-law form for the disk normal surface opacity as a function of radius. When the disk is higher inclination, it rises above the equatorial shadow and so appears brighter. Consequently, changes in inclination can be confused with variations in normal disk opacity as a function of radius. However, only limited variations in the radial disk opacity function are likely to be present, as a sharp truncation of the disk would not be consistent with the power-law form for the azimuthally averaged surface brightness profile (e.g., Fig. 5*b* of Grady et al. 2001).

Based on our exploration of models with different parameters, we have found the following. Only models with highly twisted disks have tightly wound spiral features similar to those observed. Only models with inclination increasing with radius have spiral features that extended over a sufficiently large range of azimuthal positions. Only relatively thin disks, $h/r \lesssim 0.15$, have sufficiently sharp or fine features to be similar to the observations. We find a degeneracy between the disk inclination, the angular form of attenuation from the inner disk, and the disk thickness, because these parameters all affect the contrast or amplitude of the spiral features. We did not find models with morphology similar to that observed with disks higher than $i \sim 15^\circ$ and lower than $i \sim 6^\circ$. Low-inclination disks failed to exhibit sufficiently high surface brightness variations, and high-inclination disks exhibited multiple folds along the line of sight, reducing the surface brightness variations. Models with small shadow angular scale lengths ($\theta_\tau \lesssim 5^\circ$) have dust lanes that are excessively deep, suggesting that the upper layers of the inner disk have an opacity distribution (as a function of θ) with a moderately large angular scale length.

3.2. *Mass Constraints*

By matching the observed morphology of the disk with our model, we can estimate the extent that the disk is twisted. This is described by parameters A_0 and β (see eq. [4]). We consider here the hypothesis that the twist was caused by an unseen inner planet that is misaligned with the outer disk (e.g., Mouillet et al. 1997; Augereau et al. 2001b). We remind the reader that

equation (5) refers to a tilted disk with negligible mass that is perturbed by an inner planet. The parameter A_0 depends on the time since the disk was initially tilted, Δt, and the mass and semimajor axis of the hypothetical inner planet causing the precession. We can assume that Δt is less than the age of the star or $\Delta t < 10^7$ yr. This allows us to place a lower limit on the mass of the planet times the square of the planet semimajor axis. Using equation (4) and replacing Δt with the age of the system, $t_{\rm age}$, we find

$$D^2 M_p > \frac{4|A_0| M_* r_0^{7/2}}{3\sqrt{GM_*} t_{\rm age}}. \quad (6)$$

Computing these quantities for our value of A_0 (in radians) and reference radius r_0 (listed in Table 2), we find

$$D^2 M_p \gtrsim 2.9 \times 10^4 \ {\rm AU}^2 M_J, \quad (7)$$

where M_J is the mass of Jupiter. However, this constraint is impossible to satisfy for a single Jovian mass at small radius. This constraint cannot be satisfied for a Jovian-mass planet within the lit edge of the disk at 13 AU (Grady et al. 2005). A brown dwarf–sized object at $D \sim 200$ AU would open a gap in the disk that would be observable in the images. The simplest scenario of an initially misaligned low-mass disk and a single inner planet fails to account for the twistedness of the disk.

One way to account for the highly twisted disk would be if the disk itself contained significant mass. For example, a Jovian mass of planetesimals between 100 and 200 AU but misaligned with the outer disk could account for the twisted nature of the disk. If this mass is not confined to one body but extended, then the radial power of the precession angle would be reduced. This might account for the somewhat better match of our model MB with $\beta = 2.5$ instead of 3.5. HD 100546's disk appears to be more twisted than Beta Pictoris's disk; however, Beta Pictoris is 10–20 times older, so the extent of the twist is less of a constraint on the planetary and disk system.

3.3. *Leading or Trailing Arms*

It may in future become possible to measure the sense of rotation of HD 100546's disk. The disk rotation axis could be similar to the star's rotation axis. Unfortunately, the rotation axis of the star HD 100546 is not known. Clarke et al. (1999) attempted to measure this axis from polarization measurements; however, these were affected by scattering from the surrounding dust. In spite of this, we now discuss the sense of the warp in comparison to the direction disk rotation. Future measurements of either the disk or stellar rotation could be used to support or refute dynamical explanations for the spiral morphology.

Equation (3) shows that the inner disk should precesses faster than outer disk and in the retrograde sense. Consequently, we expect the disk to twist in the direction of rotation as the radius increases. If we differentiate equation (3) we find that $d\Omega/dr$ is positive, and so Ω increases in the direction of rotation. The spiral features would be *leading* instead of trailing. If the twist is a result of precession induced by bodies in the disk interior, we would predict that the disk is rotating clockwise on the sky. We expect the northwestern side to be blueshifted from the system center of mass and the southeastern side to be redshifted. The southwestern side is probably closer to us, based on the nebulosity on the southern side seen in the STIS image (Grady et al. 2001) and because of the excess seen in the scattered near-infrared light at $r \sim 3''$ on the southern side (Augereau et al. 2001a).

4. SUMMARY AND DISCUSSION

In this paper we have presented a new model for the spiral features seen in visible scattered light images of HD 100546's disk. We reproduce the two-armed spiral features with a highly twisted warped disk model. The disk inclination with respect to the systems ecliptic is low, 6°–15°, and increasing with radius. The disk is fairly thin, with a ratio of FWHM/r of $\sim$0.15. Surface brightness variations are due to a high surface gradient with respect to the line of sight in the folds of the disk. Dark lanes increase the contrast of the spiral features and are caused by equatorial shadowing from an inner unresolved disk. As a nearly Keplerian system can maintain a warp for long periods of time (secular timescales rather than rotational periods), this model has some advantages over transient spiral models. The observed spiral features end at positions approximately located on the disk major axis (as seen on the sky). This is a feature common to moderate inclination warped disk models that would not be exhibited by a spiral density wave model for the spiral features.

However, the morphology requires the disk to be so twisted that the tidal force from a Jovian-mass object in the inner disk clearing cannot have induced the twist during the lifetime of the star. One possibility is that the disk warp could have been induced by a significant mass (Jovian mass) of objects that are inclined with respect to the outer disk, well outside the inner clearing, at intermediate radii between 100 and 200 AU.

We now discuss proposed mechanisms for accounting for the tilt between the disk and objects in the inner disk. A stellar encounter could tidally induce a tilt in the outer disk. In this case, we would expect that the disk tilt or inclination would increase with radius (e.g., as calculated by Kobayashi & Ida [2001]). Our models better match the angular extension of the spiral feature when the tilt increases with radius, suggesting that this may be the case for HD 100546's disk. Such a stellar encounter, while unlikely in the field, could have been probable in a denser stellar environment, such as the star's birth cluster. An alternative scenario is that resonances between multiple planets cause an inclination increase in one of the planets (Thommes & Lissauer 2003). In this case, the disk would have tilt or inclination that decreases with radius (Mouillet et al. 1997). Also, this model would likely require vertical resonances for planets at large semimajor axes to account for the highly twisted disk. The different dynamical scenarios predict different radial forms for the angles used to describe the warp, i and Ω. Consequently, better observations and accompanied modeling of the HD 100546's disk and other circumstellar disks will produce better constraints on the disk tilt and precession angle as a function of radius. These in turn will allow better tests of the dynamical models for the warp formation and evolution. The dynamical models have the capability of providing unique constraints on the mass distribution in the outer disk.

In this paper we have used a very simple model to take into account equatorial shadowing due to the opacity of the inner disk. Unfortunately, we find a degeneracy in our models between the disk tilt, the angular form of attenuation from the inner disk, the disk thickness, and the opacity as a function of radius. This is because these parameters all affect the surface brightness contrast or amplitude of the spiral features. Shadowing is likely to be a strong function of color; consequently, multicolor imaging may be able to probe the structure of the inner unresolved disk as well as to better constrain the geometry and structure of the

outer disk. Our model assumes an optically thin outer disk; however, the optical depth of HD 100546's outer disk has not been well constrained (Augereau et al. 2001a). Warped disks seen at visible wavelengths should exhibit asymmetries due to optical depth variations and asymmetries due to forward scattering. Both of these effects should be more severe at bluer wavelengths, providing a possible way to discriminate between geometric models. We note that some asymmetries and perceived clumps in visible light in edge-on warped disks (e.g., as seen in AU Microscopii; Liu 2004) might in future be explained with a warped disk rather than with a model containing eccentric rings. However, asymmetries observed in thermal or mid-infrared emission, such as is observed in Beta Pictoris by Telesco et al. (2005), could not be explained via a warped disk model, as at these wavelengths we expect the disks to be more nearly optically thin the emission should be nearly isotropic.

The observations of Eisner et al. (2004) suggest that He/Be stars are not highly warped. However, moderate inclination warps, such as found here, would not violate the comparison of submillimeter and near-infrared position angles and ellipticities. It is possible that highly tilted warped disks may provide alternate explanations for excess far-infrared emission in some systems, as such disks cover a larger solid angle and so can absorb more stellar flux at large radii than a coplanar disk of the same thickness.

I thank the Research School of Astronomy and Astrophysics of the Australian National University and Mount Stromlo Observatory for hospitality and support during spring 2005. Support for this work was in part provided by National Science Foundation grant AST 04-06823 and the National Aeronautics and Space Administration under grant NNG 04-GM12G, issued through the Origins of Solar Systems Program. Support was also provided by the National Science Foundation to the Kavli Institute for Theoretical Physics under grant PHY 99-07949.

REFERENCES

Ardila, D. R., et al. 2005, ApJ, 627, 986
Augereau, J. C., Lagrange, A. M., Mouillet, D., & Menard, F. 2001a, A&A, 365, 78
Augereau, J. C., Nelson, R. P., Lagrange, A. M., Papaloizou, J. C. B., & Mouillet, D. 2001b, A&A, 370, 447
Bouwman, J., de Koter, A., Dominik, C., & Waters, L. B. F. M. 2003, A&A, 401, 577
Burrows, C. J., et al. 1995, BAAS, 187, 32.05
Clarke, D., Smith, R. A., & Yudin, R. V. 1999, A&A, 347, 590
Dullemond, C. P. 2002, A&A, 395, 853
Dullemond, C. P., & Dominik, C. 2004, A&A, 417, 159
Dullemond, C. P., Dominik, C., & Natta, A. 2001, ApJ, 560, 957
Eisner, J. A., Lane, B. F., Hillenbrand, L. A., Akeson, R. L., & Sargent, A. I. 2004, ApJ, 613, 1049
Grady, C. A., Woodgate, B., Heap, S. R., Bowers, C., Nuth, J. A., III, Herczeg, G. J., & Hill, H. G. M. 2005, ApJ, 620, 470
Grady, C. A., et al. 2001, AJ, 122, 3396
Heap, S. R., Lindler, D. J., Lanz, T. M., Cornett, R. H., Hubeny, I., Maran, S. P., & Woodgate, B. 2000, ApJ, 539, 435
Kobayashi, H., & Ida, S. 2001, Icarus, 153, 416
Krist, J. E., et al. 2005, AJ, 129, 1008
Liu, M. C. 2004, Science, 305, 1442
Liu, W. M., Hinz, P. M., Meyer, M. R., Mamajek, E. E., Hoffman, W. F., & Hora, J. L. 2003, ApJ, 598, L111
Mouillet, D., Larwood, J. D., Papaloizou, J. C. B., & Lagrange, A. M. 1997, MNRAS, 292, 896
Nicholson, R. A., Bland-Hawthorn, J., & Taylor, K. 1992, ApJ, 387, 503
Pantin, E., Waelkens, C., & Lagage, P. O. 2000, A&A, 361, L9
Quillen, A. C., & Bower, G. A. 1999, ApJ, 522, 718
Quillen, A. C., Brooks, M. H., Keene, J., Sterne, D., Lawrence, C. R., & Werner, M. W. 2006, ApJ, submitted (astro-ph/0601135)
Quillen, A. C., de Zeeuw, P. T., Phinney, E. S., & Phillips, T. G. 1992, ApJ, 391, 121
Quillen, A. C., Graham, J. R., & Frogel, J. A. 1993, ApJ, 412, 550
Quillen, A. C., Varniere, P., Minchev, I., & Frank, A. 2005, AJ, 129, 2481
Steiman-Cameron, T. Y., Kormendy, J., & Durisen, R. H. 1992, AJ, 104, 1339
Telesco, C. M., et al. 2005, Nature, 433, 133
Thommes, E. W., & Lissauer, J. J. 2003, ApJ, 597, 566
Tubbs, A. D. 1980, ApJ, 241, 969
van den Ancker, M. E., The, P. S., Tjin A Djie, H. R. E., Catala, C., de Winter, D., Blondel, P. F. C., & Waters, L. B. F. M. 1997, A&A, 324, L33